

Injectable Reactive Oxygen Species-Responsive SN38 Prodrug Scaffold with Checkpoint Inhibitors for Combined Chemoimmunotherapy

Yimou Gong,^{II} Muchao Chen,^{II} Yanjun Tan, Jingjing Shen, Qiutong Jin, Wutong Deng, Jian Sun,* Chao Wang, Zhuang Liu, and Qian Chen*



Cite This: <https://dx.doi.org/10.1021/acsami.0c13943>



Read Online

ACCESS |

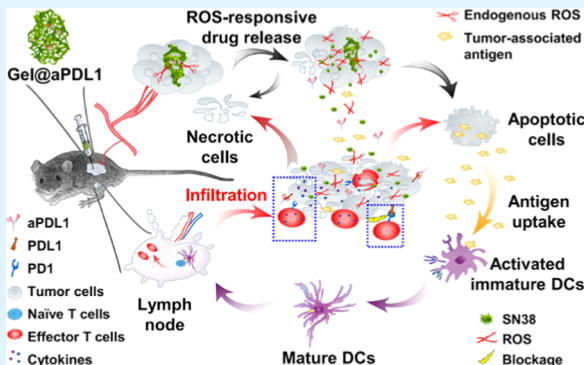
Metrics & More

Article Recommendations

Supporting Information

ABSTRACT: Chemotherapeutic agents have been widely used for cancer treatment in clinics. Aside from their direct cytotoxicity to cancer cells, some of them could activate the immune system of the host, contributing to the enhanced antitumor activity. Here, the reactive oxygen species (ROS)-responsive hydrogel, covalently cross-linked by phenylboronic acid-modified 7-ethyl-10-hydroxycamptothecin (SN38-SA-BA) with poly(vinyl alcohol) (PVA), is fabricated for topical delivery of anti-programmed cell death protein ligand 1 antibodies (aPDL1). In the presence of endogenous ROS, SN38-SA-BA will be oxidized and hydrolyzed, leading to the degradation of hydrogel and the release of initial free SN38 and encapsulated aPDL1. It is demonstrated that SN38 could elicit specific immune responses by triggering immunogenic cell death (ICD) of cancer cells, a distinct cell death pathway featured with the release of immunostimulatory damage-associated molecular patterns (DAMPs). Meanwhile, the released aPDL1 could bind to programmed cell death protein ligand 1 (PDL1) expressed on cancer cells to augment antitumor T cell responses. Thus, the ROS-responsive prodrug hydrogel loaded with aPDL1 could induce effective innate and adaptive antitumor immune responses after local injection, significantly inhibiting or even eliminating those tumors.

KEYWORDS: injectable hydrogel, SN38 prodrug, immunogenic cell death, immune checkpoint blockade, chemoimmunotherapy



1. INTRODUCTION

Chemotherapy, although not often curative, remains to be a major cancer treatment modality in clinic.¹ Recently, it has been reported that some chemotherapeutic drugs such as oxaliplatin, doxorubicin, paclitaxel, etc. apart from directly killing cancer cells, have the ability to interact with the immune system by various mechanisms.^{2–5} Chemotherapeutic drugs could induce various death modalities of cancer cells including the immunogenic cell death (ICD), which is an intrinsic cell death pathway featured with the release of damage-associated molecular patterns (DAMPs), the expression of calreticulin (CRT) on the surface of dying cells, as well as the enhanced release of ATP and high-mobility group box 1 (HMGB1).^{6–8} The overexpressed CRT would provide a signal for recruitment of dendritic cells (DCs) and promote the uptake of cancer cells.^{6,9} The released ATP and HMGB1 from cancer cells would act as an adjuvant to promote antigen presentation by antigen-presenting cells such as DCs.¹⁰ Thus, the anticancer efficacy of these chemotherapeutic drugs is partly due to the augmentation of host immune system.^{11,12}

Camptothecin (CPT), a kind of periodical antitumor alkaloid isolated from camptotheca acuminate by inhibiting

DNA replication, transcription, and mitosis, and could act as an “immunostimulant” to activate the immune system.^{9,13–16} Among various CPT derivatives, SN38 is a promising antitumor drug with high activity and efficacy, and has also been reported to effectively enhance T-cell-mediated tumor cytotoxicity.^{17–20} We hypothesized that effective delivery of SN38 to the tumor site may induce immunogenic tumor phenotype and stimulate the immune system, promising in combination with immunotherapy.

Among various mainstream immunotherapies in clinics, immune checkpoint blockade (ICB) has been witnessed to be an effective strategy to treat various malignancies.^{21–25} Recently, antibodies blocking inhibitory pathways such as cytotoxic T-lymphocyte-associated antigen 4 (CTLA4) and programmed cell death protein 1 pathway (PD-1/PD-L1) have

Received: August 3, 2020

Accepted: October 19, 2020

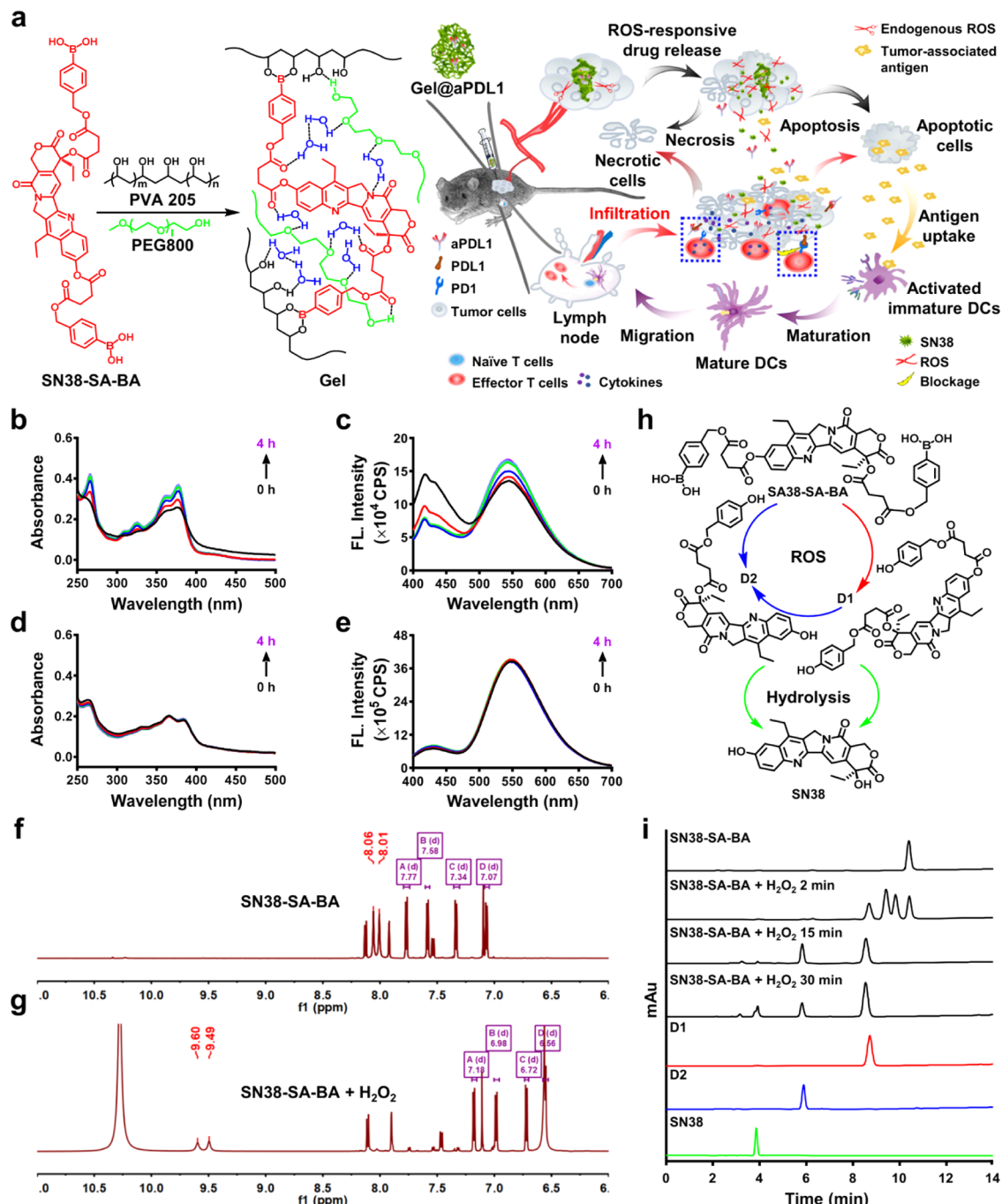


Figure 1. Scheme of injectable ROS-responsive PVA-SN38 hydrogel and characterization of SN38-SA-BA. (a) Scheme to show the formation of ROS-responsive PVA-SN38 hydrogel. (b) Time-dependent ultraviolet-visible-near-infrared (UV-vis-NIR) absorbance spectra of SN38-SA-BA (2.5 μ M) and (d) SN38 (2.5 μ M) in solution with 1 mM H₂O₂. (c) The corresponding fluorescence intensity changes of SN38-SA-BA and (e) SN38 in the presence of H₂O₂ (37 °C, $\lambda_{\text{ex}} = 365$ nm, slit width = 3/3). (f) In situ ¹H NMR spectrum of SN38-SA-BA dispersed in DMSO-d₆ solution without or (g) with H₂O₂. (h) The proposed activation modes of SN38-SA-BA in the presence of ROS. (i) High-performance liquid chromatogram (HPLC) of SN38-SA-BA recorded at different time intervals with addition of H₂O₂.

been approved by the Food and Drug Administration for cancer treatment in clinics.^{26,27} However, only a small proportion of patients (~20%) with immunogenic tumors have responses to ICB. Furthermore, ICB by activating nonspecific immune response also has been associated with various side effects including the risk of autoimmune diseases.²⁸ Therefore, the combination of SN38 and ICB may be a promising strategy for cancer treatment. However, considering the different physicochemical properties of

chemotherapeutic drugs and antibodies, how to realize synergistic therapeutic efficacy by simultaneous administration of different drugs may be an important issue in both fundamental research and clinical practice.

Hydrogel is a highly appealing drug delivery system, allowing locally controlled and sustainable release of hydrophilic and hydrophobic drugs.²⁹ For local delivery system, the bioavailability of drug is increased and the side effects associated with the off-target of drugs would be minimized.^{30,31} Herein, we

designed the ROS-responsive hydrogel via covalently cross-linking poly(vinyl alcohol) (PVA) with phenylboronic acid-modified SN38 (SN38-SA–BA) for local delivery of aPDL1 and demonstrated the high efficacy of this two-component system in stimulating immune system and inhibiting tumor growth (Figure 1a). We found that the injectable ROS-responsive hydrogel could be gradually degraded in the tumor microenvironment (TME) owing to the presence of endogenous ROS and released effective chemotherapeutic drug, SN38, which may stimulate the production of more ROS and trigger the further release of SN38 via a positive feedback manner.³² Subsequently, the released SN38 could trigger the programmed cell death by releasing DAMPs including the CRT exposure, HMGB1 release, ATP secretion, and heat shock protein 70 kDa (HSP70) expression, which together would activate the immune system and trigger antitumor immune responses. Meanwhile, the simultaneously released aPDL1 preloaded in the hydrogel could block the PD-1/PD-L1 pathway to facilitate T-cell-mediated immune responses to attack tumor cells. Thus, the ROS-responsive hydrogel caused an immunogenic tumor phenotype via the self-accelerated release of chemotherapeutic drug and promoted immune response rates of aPDL1, achieving synergistic chemoimmunotherapy in the B16F10 melanoma tumor model.

2. EXPERIMENTAL SECTION

2.1. Materials. 4-(Hydroxymethyl)benzeneboronic acid pinacol ester (BP), succinic anhydride (SA), and sodium periodate (NaIO_4) were purchased from Energy Chemical. 4-Dimethylaminopyridine (DMAP) and bovine serum immunoglobulin G (IgG) were obtained from Sigma-Aldrich. Anhydrous tetrahydrofuran (THF), anhydrous chloromethane (DCM), poly(ethylene glycol)-800 (PEG800), and 7-ethyl-10-hydroxycamptothecin (SN38) were purchased from 3A Chem. *N,N'*-Diisopropylcarbodiimide (DIC) was applied from Adamas. Poly(vinyl alcohol) 0588 low-viscosity (PVA 20S or PVA) was purchased from Aladdin. Cyanine 5.5 monosuccinimidyl ester (Cys5.5-NHS) was purchased from AAT Bioquest, Inc. All of the other organic solvents were purchased from Enox (Chinasun Specialty Products Co., Ltd.) and used as received.

2.2. Characterizations. An NMR spectrometer (Bruker 600) and a mass spectrometer (Bruke P-SIMS-Gly FT-ICR) were applied to characterize the synthesized molecular structure. HPLC analyses were performed on an Agilent 1100 instrument equipped with a reversed-phase column (Kromasil C18, 250 × 4.6 mm²). The eluent used for analysis was a water–methanol gradient (0–5 min, water 30%; 5–20 min, water 10%). The injection volume of the dilute sample was 2 μL . The flow rate was set as 0.8 mL/min. The absorption of samples was recorded by a UV–vis spectrometer at 230 nm. Time-dependent UV–vis–NIR absorbance spectrum and the fluorescence intensity were recorded using a UV–vis–NIR spectrophotometer (GENESYS 10S, Thermo Fisher) and a fluorescence spectrometer (Aqualog, HORIBA; $\lambda_{\text{ex}} = 365$ nm, slit width = 3/3), respectively.

2.3. Synthesis of ROS-Responsive Prodrug. **2.3.1. Synthesis of SA–BP.** SA (1.71 g, 17.09 mmol) was added to a stirred mixture of BP (2.0 g, 8.54 mmol) and DMAP (52 mg, 0.43 mmol) in anhydrous THF (35 mL). Subsequently, the mixture was stirred at ambient condition for 36 h, followed by the addition of methanol (10 mL) to deplete the excess SA. Then, the residue was obtained by the evaporation of the reaction solvent, and dissolved in DCM. The DCM phase was further washed with 0.1 M HCl, water, and brine in sequence. Next, after removal of moisture by anhydrous Na_2SO_4 , the DCM phase was evaporated via reduced pressure to obtain SA–BP (2.8 g, 95% yield). ¹H NMR (600 MHz, CDCl_3) δ (ppm): 7.80 (d, $J = 7.8$ Hz, 2H), 7.34 (d, $J = 7.8$ Hz, 2H), 5.16 (s, 2H), 2.73–2.66 (m, 4H), 1.34 (s, 12H).

2.3.2. Synthesis of SN38-SA–BP. SN38 (392 mg, 1 mmol) and SA–BP (1.03 g, 3 mmol) were dispersed in 30 mL of anhydrous

DCM at 0 °C. Followed by the addition of DMAP (61 mg, 0.5 mmol) and DIC (465 μL , 3 mmol), the intermixture was stirred at ambient condition overnight. Next, after filtering out the precipitate, the filtrate was evaporated via reduced pressure and further purified via column chromatography (hexane/ethyl acetate = 1/1) on silica gel to provide SN38-SA–BP as a pale white solid (480 mg, 46% yield). ¹H NMR (600 MHz, $\text{DMSO}-d_6$) δ (ppm): 8.10 (d, $J = 9.1$ Hz, 1H), 7.92 (s, 1H), 7.66 (d, $J = 7.7$ Hz, 2H), 7.48 (d, $J = 7.7$ Hz, 2H), 7.43 (dd, $J = 9.1, 1.7$ Hz, 1H), 7.39 (d, $J = 7.7$ Hz, 2H), 7.13 (d, $J = 7.7$ Hz, 2H), 7.07 (s, 1H), 5.51 (s, 2H), 5.23 (ABq, $\Delta\delta_{\text{AB}} = 0.06$, $J_{\text{AB}} = 18.5$ Hz, 2H), 5.18 (s, 2H), 5.12 (ABq, $\Delta\delta_{\text{AB}} = 0.02$, $J_{\text{AB}} = 13.4$ Hz, 2H), 3.15–3.06 (m, 2H), 2.97 (t, $J = 6.3$ Hz, 2H), 2.92–2.87 (m, 1H), 2.83 (t, $J = 6.4$ Hz, 2H), 2.81–2.76 (m, 1H), 2.71–2.64 (m, 2H), 2.16–2.09 (m, 2H), 1.27 (s, 24H), 1.25 (t, $J = 7.6$ Hz, 3H), 0.91 (t, $J = 7.3$ Hz, 3H). ¹³C NMR (151 MHz, $\text{DMSO}-d_6$) δ (ppm): 171.7, 171.2, 171.1, 170.9, 167.1, 156.4, 151.7, 149.0, 146.4, 146.2, 145.3, 145.1, 139.3, 134.5, 134.2, 131.1, 128.3, 127.1, 127.0, 126.5, 125.3, 118.7, 115.0, 95.0, 83.6, 76.0, 66.3, 65.5, 65.3, 49.4, 30.3, 29.0, 28.7, 28.6, 28.5, 24.6, 22.2, 13.7, 7.5. HRMS (m/z , ESI): calcd for $\text{C}_{56}\text{H}_{62}\text{B}_2\text{N}_2\text{O}_{15}$: 1024.4336, found: 1025.4446 [M + H]⁺.

2.3.3. Synthesis of SN38-SA–BA. HCl (1 M, 700 μL) was added dropwise to a mixed solution of 15 mL of THF/H₂O (V/V = 4/1) containing SN38-SA–BP (480 mg, 0.468 mmol) and NaIO_4 (598 mg, 2.81 mmol) at 0 °C. After that, the obtained intermixture was stirred at ambient temperature overnight. Followed by the addition of 0.01 M HCl, ethyl acetate (EA) was utilized to extract the targeted substance from the reaction mixture. Next, the EA phase was washed with water and brine. After removal of moisture by anhydrous Na_2SO_4 , the EA phase was evaporated via reduced pressure to obtain the crude product. Finally, the crude product was further pulped with the mixture of EA and hexane (EA/hexane = 1/2) to obtain SN38-SA–BA as a yellow powder (320 mg, 80% yield). ¹H NMR (600 MHz, $\text{DMSO}-d_6$) δ (ppm): 8.13 (d, $J = 9.1$ Hz, 1H), 8.04 (s, 2H), 7.99 (s, 2H) 7.93 (d, $J = 2.3$ Hz, 1H), 7.78 (d, $J = 8.0$ Hz, 2H), 7.60 (d, $J = 8.0$ Hz, 2H), 7.54 (dd, $J = 9.1, 2.3$ Hz, 1H), 7.34 (d, $J = 7.9$ Hz, 2H), 7.09 (s, 1H), 7.08 (d, $J = 7.9$ Hz, 2H), 5.51 (s, 2H), 5.26 (ABq, $\Delta\delta_{\text{AB}} = 0.04$, $J_{\text{AB}} = 18.5$ Hz, 2H), 5.16 (s, 2H), 5.11 (ABq, $\Delta\delta_{\text{AB}} = 0.03$, $J_{\text{AB}} = 12.9$ Hz, 2H), 3.15–3.07 (m, 2H), 2.98 (t, $J = 6.5$ Hz, 2H), 2.92–2.88 (m, 1H), 2.83 (t, $J = 6.6$ Hz, 2H), 2.80–2.75 (m, 1H), 2.70–2.64 (m, 2H), 2.17–2.09 (m, 2H), 1.25 (t, $J = 7.6$ Hz, 3H), 0.90 (t, $J = 7.4$ Hz, 3H). ¹³C NMR (151 MHz, $\text{DMSO}-d_6$) δ (ppm): 171.8, 171.3, 171.1, 171.0, 167.2, 156.5, 151.7, 149.1, 146.4, 146.3, 145.3, 145.2, 137.7, 134.2, 133.9, 131.1, 128.4, 127.0, 126.7, 126.2, 125.4, 118.7, 115.1, 95.1, 76.0, 66.3, 65.7, 65.5, 49.4, 30.3, 29.0, 28.7, 28.6, 22.2, 13.8, 7.5. HRMS (m/z , ESI): calcd for $\text{C}_{44}\text{H}_{42}\text{B}_2\text{N}_2\text{O}_{15}$: 860.2771. Found: 861.2866 [M + H]⁺, 883.2677 [M + Na]⁺.

2.4. ROS-Responsive Behavior of Prodrug. To a stirred solution of SN38-SA–BA (172 mg, 0.2 mmol) in acetonitrile (20 mL, containing 5% DMSO), H_2O_2 (30%, 0.5 mL) was added. The reaction process was monitored via high-performance liquid chromatography (HPLC) at different time intervals. The intermixture was agitated at ambient temperature for 1 h. After removal of acetonitrile by evaporation, EA was added. Subsequently, the EA phase was washed with water and brine. Next, anhydrous Na_2SO_4 was added to the EA phase to get rid of the moisture. Then, after removing the desiccant by filtration, the EA phase was concentrated and further purified by column chromatography (DCM/EA = 3/2) on silica gel to obtain the major intermediate D1 and the minor intermediate D2.

Intermediate D1 (two isomers), ¹H NMR (400 MHz, $\text{DMSO}-d_6$) δ (ppm): 9.52 (s, 1H), 9.43 (s, 1H), 8.14 (d, $J = 8.2$ Hz, 1H), 7.95 (s, 1H), 7.50 (d, $J = 7.4$ Hz, 1H), 7.20 (d, $J = 6.0$ Hz, 2H), 7.10 (s, 1H), 7.03 (d, $J = 6.0$ Hz, 2H), 6.74 (d, $J = 6.1$ Hz, 2H), 6.59 (d, $J = 6.1$ Hz, 2H), 5.50 (s, 2H), 5.31 (s, 2H), 5.02 (s, 2H), 4.96 (m, 2H), 3.15 (s, 2H), 2.94 (s, 2H), 2.90–2.76 (m, 4H), 2.61 (s, 2H), 2.11 (s, 2H), 1.27 (s, 3H), 0.89 (s, 3H). ¹³C NMR (151 MHz, $\text{DMSO}-d_6$) δ (ppm): 173.0, 171.4, 171.0, 167.2, 157.3 (157.2), 156.7 (156.5), 149.4, 148.6, 146.8 (146.7), 145.3 (145.2), 144.3, 143.8 (143.6), 142.7, 131.4 (131.2), 130.1, 129.9, 129.8, 129.2, 128.9, 128.2, 127.9 (127.8), 126.6, 126.1, 122.7 (122.4), 121.7 (121.4), 117.9 (117.7),

115.2 (115.1), 114.9, 104.8, 103.6, 94.5 (94.2), 76.0, 69.9, 66.3, 65.8, 49.4, 30.2, 28.8, 28.6, 22.3, 13.3, 7.5. HRMS (*m/z*, ESI): calcd for C₄₄H₄₀N₂O₁₃: 804.2530. Found: 805.2624 [M + H]⁺, 827.2445 [M + Na]⁺.

Intermediate D2. ¹H NMR (600 MHz, DMSO-*d*₆) δ (ppm): 10.30 (s, 1H), 9.42 (s, 1H), 7.97 (d, *J* = 8.9 Hz, 1H), 7.38 (m, 2H), 7.04 (d, *J* = 8.4 Hz, 2H), 7.00 (s, 1H), 6.60 (d, *J* = 8.4 Hz, 2H), 5.48 (s, 2H), 5.26 (s, 2H), 4.97 (ABq, $\Delta\delta_{AB}$ = 0.05, *J_{AB}* = 11.9 Hz, 2H), 3.07 (q, *J* = 7.6 Hz, 2H), 2.87–2.81 (m, 1H), 2.75–2.70 (m, 1H), 2.61–2.58 (m, 2H), 2.12–2.05 (m, 2H), 1.28 (t, *J* = 7.4 Hz, 3H), 0.88 (t, *J* = 7.5 Hz, 3H). ¹³C NMR (151 MHz, DMSO-*d*₆) δ (ppm): 171.4, 171.0, 167.2, 157.2, 156.7, 156.6, 148.7, 146.8, 145.4, 143.6, 142.7, 131.4, 129.8, 129.6, 128.2, 127.9, 126.1, 122.4, 117.7, 114.9, 104.8, 94.3, 76.0, 66.3, 65.8, 49.4, 30.2, 29.0, 28.8, 28.6, 22.3, 13.3, 7.5. HRMS (*m/z*, ESI): calcd for C₃₃H₃₀N₂O₉: 598.1951. Found: 599.2028 [M + H]⁺, 621.1845 [M + Na]⁺.

2.5. Fabrication and Characterization of PVA-SN38 Hydrogel. Followed by the addition of PVA (0.5 g) to deionized water (5 mL), the suspension mixture was agitated at 90 °C to acquire a clear solution A (wt %, 10%). SN38-SA–BA (40 mg) was dissolved in 800 μ L of PEG800 to obtain solution B (50 mg/mL). Following Table S1, component part I and part II were prepared. Next, the two components were mixed and recorded via a digital camera.

A representative PVA-SN38 hydrogel used for further characterization was prepared by mixing PVA (7.5 wt % in PBS, pH 7.4, 200 μ L) and SN38-SA–BA (20 mg/mL, in PEG800, 100 μ L). To be applied *in vivo*, PVA and SN38-SA–BA solutions were mixed in syringes and injected into the tumor directly to fabricate a hydrogel *in situ*. Next, a scanning electron microscope (SEM, Gemini 500, Zeiss) was used to characterize the surface morphology of the hydrogel. Then, rheology experiments were performed on a rheometer (HAAKE Mars 40, Thermo Fisher; Rotor, P20/Ti; gap, 0.75 mm; temp, 37 °C). Moreover, a confocal laser scanning microscope (CLSM, LSM 800, Zeiss) was used for characterization of the distribution of antibodies in gel. Furthermore, the ROS-sensitive release profiles of SN38 and antibodies were determined by HPLC and Bovine Immunoglobulin G ELISA Kit (Abcam, Catalog: 205078), respectively.

2.6. In Vitro Experiment. Murine melanoma B16F10 cells were obtained from the Cell Bank of Type Culture Collection of Chinese Academy of Sciences (Shanghai, China) and cultured according to standard protocol. To evaluate the cytotoxicity of SN38 and SN38-SA–BA, the B16F10 cells were incubated with various concentrations of SN38 and SN38-SA–BA (dissolved in PEG800) for 24 h. The relative cell viabilities were measured via the MTT assay.

To investigate the ICD of cancer cells, the B16F10 cells were seeded into 24-well chambered slides (5 × 10⁴ cells/well, 1 mL system) and cultured overnight. H₂O₂ was added to maintain an oxidative stress (50 μ M/well). Then, cancer cells were incubated with PBS (30 μ L/well), PVA&PEG800 (7.5% PVA in PBS, 20 μ L/well; PEG800, 10 μ L/well), SN38 (1 mg/mL SN38 in PEG800, 10 μ L/well), or PVA-SN38 hydrogel (prepared in transwells, 7.5% PVA in PBS, 20 μ L/well; 2.2 mg/mL SN38-SA–BA in PEG800, 10 μ L/well). Gel pieces were pretreated with PBS containing H₂O₂ (5 mM, 30 μ L) for 20 min to induce gel degradation before addition to the cells. After 4 h incubation, the cells were stained with anti-calreticulin antibody or anti-HMGB1 antibody for confocal imaging. Meanwhile, the cell culture supernatant was collected to measure the concentration of ATP using an ATP assay kit (S0026, Beyotime Biotechnology). Moreover, the calreticulin expression content of cancer cells was further measured by flow cytometry (C6 Plus, BD Accuri).

2.7. In Vivo Tumor Models and Treatment. Age-matched female C57B6 mice (6–8 weeks) obtained from Soochow University Laboratory Animal Center were used throughout all animal experiments under appropriate protocols, which were carried out according to the guidelines for institutional committee for animal use and care regulations. For B16F10 melanoma tumor model, B16F10 cells (2 × 10⁶ cells/mouse) were subcutaneously implanted into the right backside of each mouse. The tumors' size was calculated as (long

diameter × short diameter²)/2 using the diameters of the tumor measured with a digital caliper.

To study the immune responses induced by PVA-SN38 hydrogel *in vivo*, the mice were divided into four groups (*n* = 4) randomly and intratumorally (i.t.) injected with different formations as follows: (1) Untreated; (2) PVA&PEG800 (7.5% PVA in PBS, 20 μ L; PEG800, 10 μ L); (3) SN38 (7.6 mg/mL in PEG800, 30 μ L); and (4) Gel (7.5% PVA in PBS, 20 μ L; 50 mg/mL SN38-SA–BA in PEG800, 10 μ L). Five days after different treatments, the tumors and peritumor lymph nodes were obtained for further analysis by immunofluorescence staining or flow cytometry.

For combined therapy, the mice were divided into four groups (*n* = 5) randomly and i.t. injected with different formations as follows: (1) Untreated; (2) Gel (PVA, 7.5% in PBS, 20 μ L; SN38-SA–BA, 50 mg/mL in PEG800, 10 μ L); (3) aPDL1 (Catalog: BE0101, 65 μ g, in 30 μ L PBS); and (4) Gel@aPDL1 (aPDL, 65 μ g; 7.5% PVA in PBS, 20 μ L; SN38-SA–BA, 50 mg/mL in PEG800, 10 μ L). Tumor size and body weight were monitored every 2 days. After 30 days, the mice treated with Gel@aPDL1 were sacrificed, and their major organs were dissected for hematoxylin and eosin (H&E) staining and imaged by a digital microscope (80i, Nikon).

2.8. Immunofluorescence Analysis by Confocal Microscopy.

Tumor slices were prepared using the cryotome (CM1806, Leica) and mounted on slides. After being fixed with ice-cold acetone, the slices were washed with PBS. Next, they were blocked with BSA (3%) and stained with primary antibodies overnight at 4 °C. After being washed with PBS, the tumor slices were further stained with a fluorescence-labeled secondary antibody (goat anti-rabbit IgG H&L, Alexa Fluor 488) for 90 min. After staining with DAPI, the slides were imaged by CLSM. Primary antibodies: CellROX Oxidative Stress Reagents (Thermo Fisher, Catalog: C10444), anti-calreticulin antibody (Abcam, UK), anti-HMGB1 antibody (Abcam, UK), and anti-HSP70 antibody (Abcam, UK). The relative quantification of fluorescence was analyzed with ImageJ software.

2.9. Flow Cytometry. To study the immune cells in the lymph nodes or tumors of mice in different groups, homogenized tissues' single-cell suspension was obtained according to the well-established protocol. Then, the cells were stained with CellROX Oxidative Stress Reagents (Thermo Fisher, Catalog: C10444) or fluorescence-labeled antibodies: CD11c (Catalog: 117310), CD80 (Catalog: 104708), CD86 (Catalog: 105114), CD45 (Catalog: 103108), CD3 (Catalog: 100204), CD4 (Catalog: 1004112), CD11b (Catalog: 101208), CD8a (Catalog: 100732), and Ki67 (Catalog: 652409). A total of 1 × 10⁶ events in ungated flowchart in each sample were collected using a flow cytometer (C6 Plus, BD Accuri) and analyzed by FlowJo software (Ver.10.0.7). All of the antibodies used except as additionally mentioned were purchased from Biolegend (San Diego, California).

2.10. Cytokine Detection. The supernatants of homogenized tumor tissues were isolated from the mice in different groups and diluted for analysis. According to vendors' instructions, enzyme-linked immunosorbent assay (ELISA) kits of TNF- α (Dakewe Biotech) or IFN- γ (Dakewe Biotech) were utilized to measure the content of the TNF- α or IFN- γ in tumor tissues, respectively.

3. RESULTS AND DISCUSSION

3.1. Synthesis of ROS-Responsive Prodrug. The ROS-responsive prodrug SN38-SA–BA containing double phenylboronic acid groups at its core structure positions 10 and 20 was synthesized as shown in Scheme S1.³³ First, SA–BP was synthesized via the acylation reaction between BP and SA. The intermediate, SN38-SA–BP, was obtained by esterification between SA–BP and SN38 in the solution of DIC/DMAP. Then, the final drug cross-linker SN38-SA–BA was obtained by removing pinacol protection of SN38-SA–BP in NaIO₄/1 M HCl system.³⁴ All of the intermediates and products were characterized by standard analytical means (Figures S6–S10, S15, and S16).

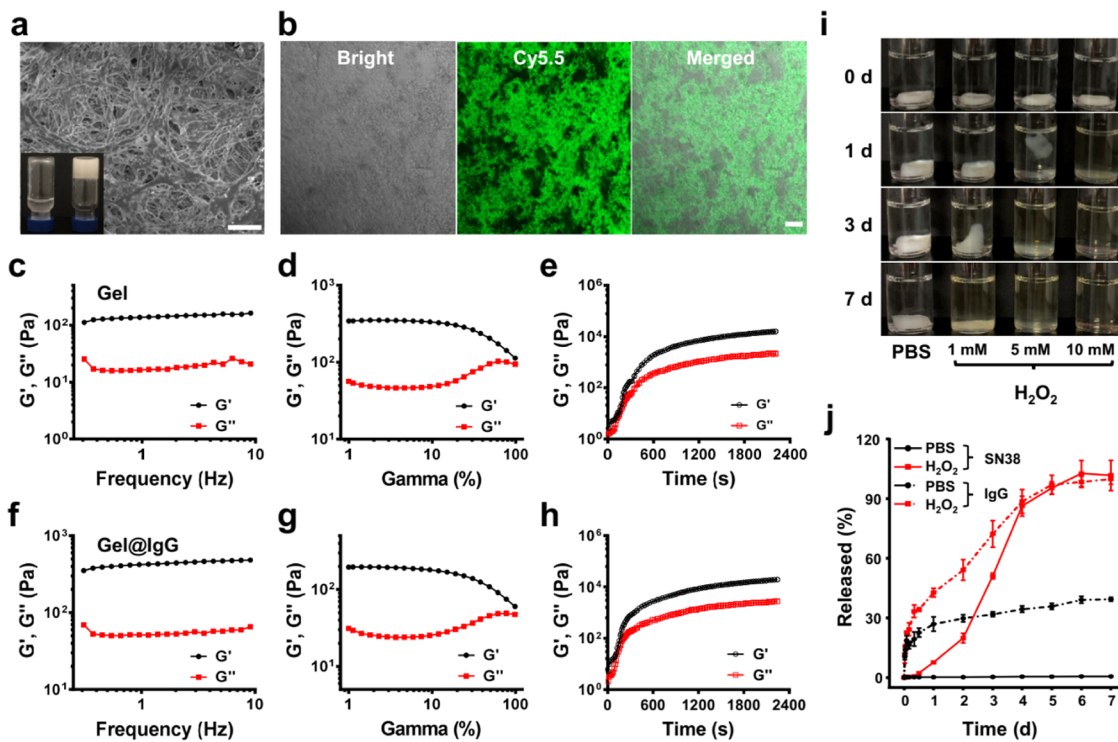


Figure 2. Characterization of PVA-SN38 hydrogel. (a) Representative SEM image of PVA-SN38 hydrogel. Scale bar, 10 μm . Inset: photographs of the PVA/PEG800 mixture without (left) or with (right) adding SN38-SA-BA. (b) Representative confocal images of the frozen section of Gel@IgG-Cy5.5. Scale bar, 20 μm . (c–h) Rheology behaviors of blank gel and Gel@IgG samples. (c) Frequency spectra of the elastic (G') and viscous (G'') moduli of Gel and (f) Gel@IgG. (d) Strain spectra of the G' and G'' moduli of Gel and (g) Gel@IgG. (e) Evolution of G' and G'' over time for Gel and (h) Gel@IgG. Experiments were performed at a constant frequency of 1 Hz. (i) Morphology changes of gels in PBS (pH 7.4) with different H_2O_2 concentrations at 37 °C over time. (j) Cumulative release profiles of SN38 and IgG from Gel@IgG when incubated with 1 mM H_2O_2 . The liberated SN38 was analyzed by HPLC, and the released antibody was determined by ELISA. IgG was used as the surrogate of aPDL1 (300 μg per sample). Data are shown as mean \pm s.e.m. ($n = 3$).

To verify the ROS-responsive behavior of the synthesized prodrug, SN38-SA-BA and free SN38 were incubated in PBS (pH = 7.4) containing 1 mM H_2O_2 , and measured by UV-vis–NIR absorption and fluorescence spectra. As we expected, the absorption and fluorescence of SN38-SA-BA increased in PBS containing H_2O_2 (Figure 1b,c), while the absorption and fluorescence of SN38 were stable in the same condition (Figure 1d,e). To investigate the degradation process, in situ nuclear magnetic resonance (NMR) spectrum analysis of SN38-SA-BA was carried out. In the NMR spectrum, the characteristic resonance signals of boronic acid (δ 8.06, 8.01 ppm) disappeared and new resonance signals (δ 9.60, 9.49 ppm) appeared in solution containing H_2O_2 (Figures 1f,g and S1a,b). Meanwhile, the resonance signals of spin protons on the benzene ring of phenylboronic acid moved from low field (δ 7.77, 7.58, 7.34, 7.07 ppm) to high field (δ 7.18, 6.98, 6.72, 6.56 ppm, Figures 1f,g and S1a,b). The same signals (δ 9.59, 9.49 ppm) were also observed for SN38-SA-BP under the same condition, together with the pinacol methyl group with one peak (δ 1.27 ppm) changed to two peaks (δ 1.13 and 1.06 ppm) and the chemical shift of hydrogen nucleus on the benzene ring of phenylboronic acid also moved from low field (δ 7.66, 7.48, 7.39, 7.13 ppm) to high field (δ 7.17, 6.98, 6.72, 6.55 ppm, Figure S1d,e). These results indicated that the B–C bonds of SN38-SA-BA(BP) were broken and the phenolic hydroxyl groups of intermediate D1 (Figures 1h and S1c) were formed in oxidative stress. Moreover, intermediate D1 was the major degradant isolated by column chromatography, and the intermediate D2 (Figure 1h) was the minor degradant of

SN38-SA-BA. The degradant chemical components were further confirmed by NMR analysis (Figures S1c and S11–S14) and electrospray ionization high-resolution mass spectroscopy (ESI-HRMS, Figures S17 and S18). Furthermore, the degradation of SN38-SA-BA was further characterized by high-performance liquid chromatography (HPLC) (Figure 1i). It was found that SN38-SA-BA (retention peak at 10.4 min) could be directly decomposed into major intermediate D1 (retention peak at 8.7 min) and minor intermediate D2 (retention peak at 5.8 min), and the intermediate D1 could be further gradually oxidized to intermediate D2. Moreover, both intermediate D1 and intermediate D2 could be hydrolyzed to SN38 (retention peak at 3.9 min) (Figure 1h,i).³³

3.2. Formation of ROS-Responsive Hydrogel. Encouraged by the ROS-responsive prodrug linker, we next explored whether it could be used to fabricate hydrogel. SN38-SA-BA containing two phenylboronic acids could be dispersed in PEG800, which is the suitable solution for prodrug linkers, and then it was mixed with PVA solution with different volume ratios (Table S1). As shown in Figure S2, the mixtures of PVA (7.5 wt % in H_2O , 200 μL) and SN38-SA-BA (2.2–50 mg/mL, in PEG800, 100 μL) could form gel quickly. Next, the macroscopic sol–gel transition was observed by mixing PVA (7.5 wt % in PBS, pH 7.4, 200 μL) and SN38-SA-BA (20 mg/mL, in PEG800, 100 μL) (Figure 2a, inset), which was further confirmed by rheological behavior test with a rapidly increased elastic modulus (G')^{24,35} (Figure 2c–e). Moreover, the formed hydrogel with porous structure was observed by SEM imaging (Figure 2a).

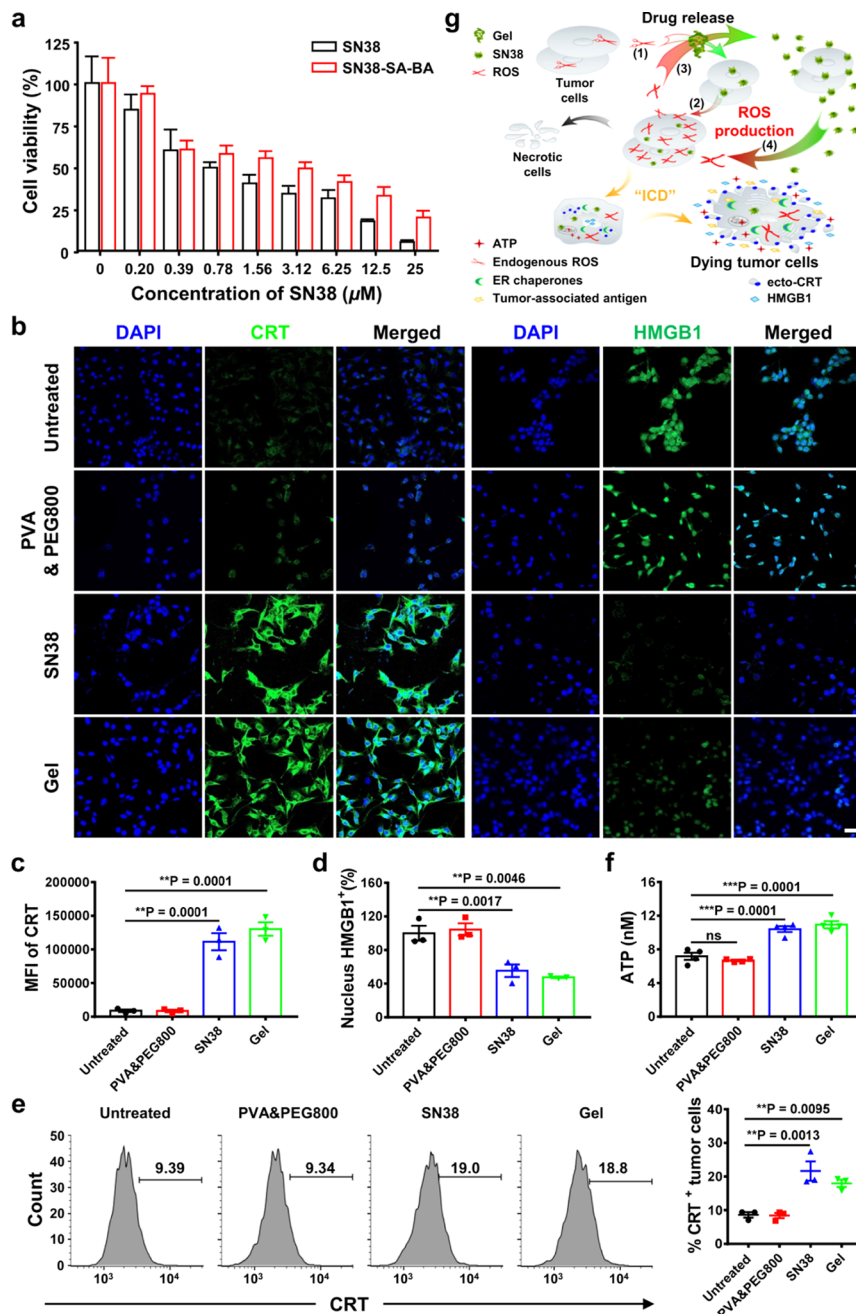


Figure 3. In vitro ICD triggered by SN38-borate hydrogel. (a) Cytotoxicity of SN38 and SN38-SA-BA against B16F10 cells after incubation for 24 h. Data are shown as mean \pm s.e.m. ($n = 6$). (b) Immunofluorescent imaging of CRT and HMGB1 expressions on B16F10 tumor cells after different treatments. Scale bar, 50 μm . (c, d) Relative semiquantification of the expression of CRT (c) and the released HMGB1 (d) according to the immunofluorescence staining images of cancer cells in (b). Data are shown as mean \pm s.e.m. ($n = 3$). (e) Representative fluorescence activated cell sorting analysis (FACS) plots (left) and the corresponding percentage (right) of the expression of CRT in tumor cells. Data are shown as mean \pm s.e.m. ($n = 3$). (f) Quantitative examination of the release of ATP from tumor cells. Data are shown as mean \pm s.e.m. ($n = 4$). (g) Proposed illustration about self-accelerated release of SN38 with ROS regeneration and inducing ICD-associated DAMPs from dying tumor cells: (1) endogenous ROS triggered the release of activated SN38; (2) the released SN38 stimulated the further production of ROS; (3) the ROS elicited the release of SN38 with high dosage; then (4) the burst of ROS and the released SN38 could induce the ICD of cancer cells. (Abbreviations: ecto-CRT, calreticulin found on the plasma membrane of viable cells; HMGB1, high-mobility group protein B1; ER, endoplasmic reticulum). Statistical significance was calculated by one-way ANOVA with Tukey's post test. * $P < 0.05$; ** $P < 0.01$; *** $P < 0.001$; ns, not significant.

Then, the IgG, a surrogate for aPDL1, was encapsulated into the PVA-SN38 hydrogel, which showed similar rheology properties to the blank hydrogel (Figure 2f-h), illustrating that the encapsulated antibodies exhibited no obvious influence on the formation of hydrogel. To investigate the distribution of antibodies in the hydrogel, Cyanine 5.5

(Cy5.5)-labeled IgG was loaded into the scaffold for confocal imaging. As we expected, Cy5.5 fluorescence with uniform distribution was observed in the frozen section of hydrogel (Figure 2b). Considering the ROS-responsive property of SN38-SA-BA, we further studied the degradability of hydrogel in PBS containing different concentrations of H_2O_2 at 37 °C.

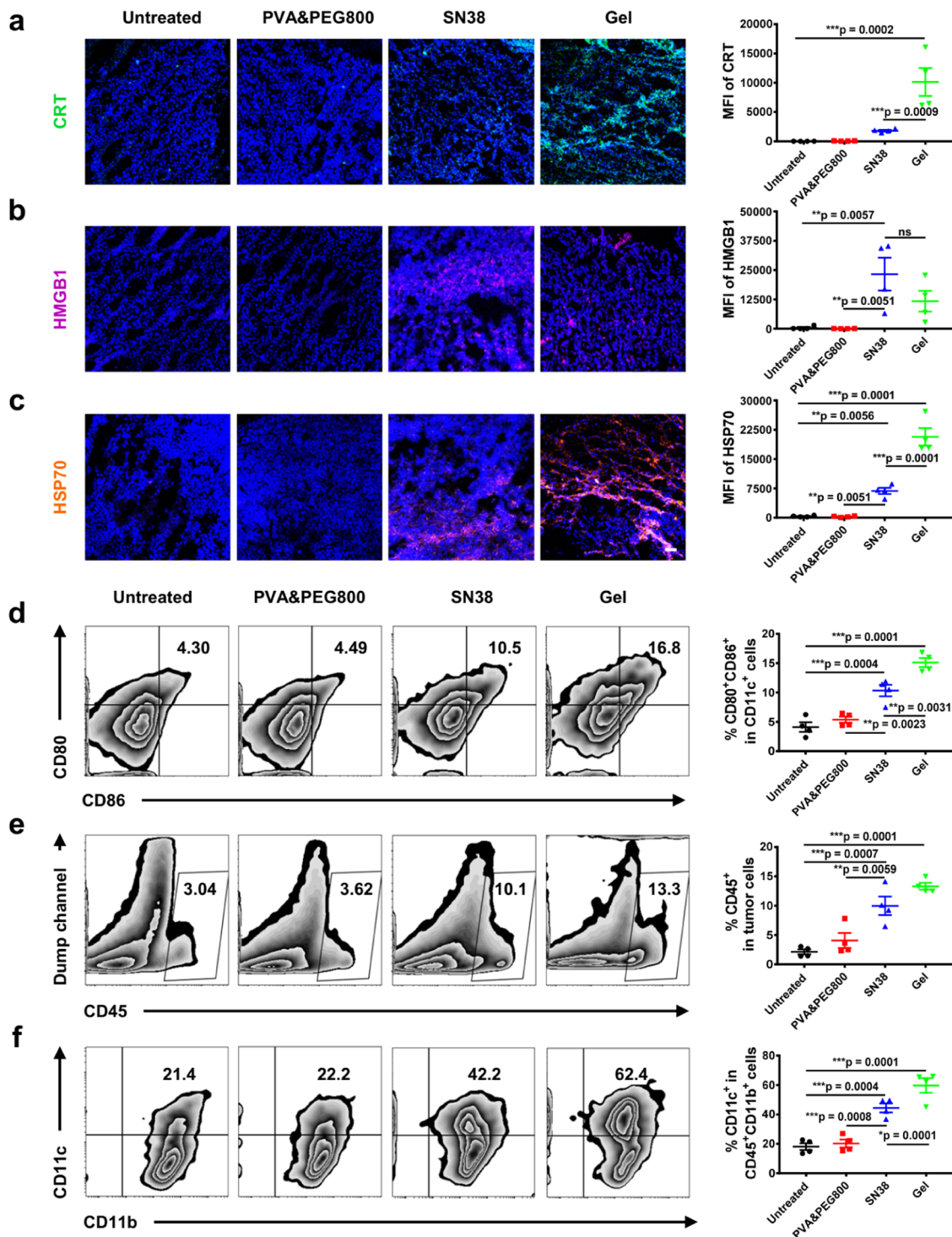


Figure 4. Immune responses induced by PVA-SN38 hydrogel in vivo. (a–c) Representative confocal images and relative semiquantification of the expression of (a) CRT, (b) HMGB1, and (c) HSP70. DAPI, blue color. Scale bar, 50 μ m. (d) Representative FACS plots (left) and the corresponding percentages (right) of CD80⁺CD86⁺ dendritic cells in peritumor lymph nodes. (e) Representative FACS plots (left) and the corresponding percentages (right) of leukocyte common antigen CD45⁺ cells in tumor. (f) Representative FACS plots (left) and the corresponding percentages (right) of CD11c⁺ DCs, gated on CD45⁺CD11b⁺ cells in tumor tissues. Data are shown as mean \pm s.e.m. ($n = 4$). Statistical significance was calculated by one-way ANOVA with Tukey's post test. * $P < 0.05$; ** $P < 0.01$; *** $P < 0.001$; ns, not significant.

Morphological changes of PVA-SN38 hydrogel were observed with the H₂O₂ concentration-dependent relationship over time (Figure 2i). Moreover, the ROS-sensitive release profiles of SN38 and IgG (aPDL1 succedaneum) were evaluated by HPLC and ELISA, respectively (Figure 2j). As expected, while small amounts of IgG could be detected in PBS, both SN38

and IgG could be quickly released from the hydrogel dispersed in the H₂O₂ solution.

3.3. Immune Responses Induced by PVA-SN38 Hydrogel. ICD is a distinct cell death pathway, which can initiate effective immune responses to attack cancer cells.⁸ Although some chemotherapeutic drugs have been reported to

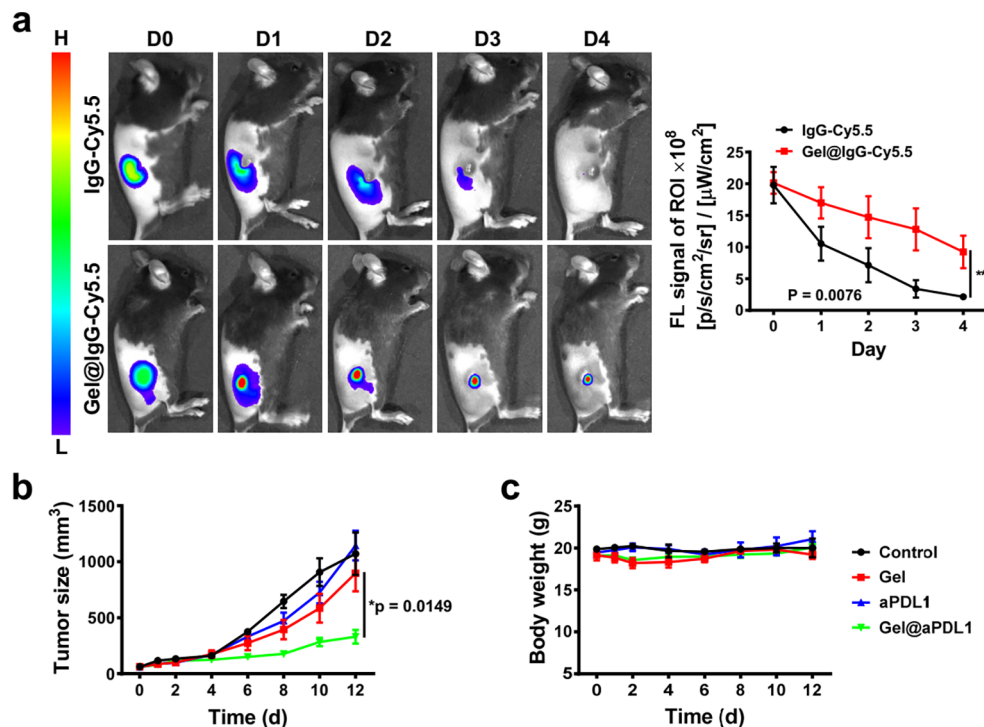


Figure 5. Combination therapy to inhibit the growth of B16F10 melanoma tumors. (a) Left, in vivo representative fluorescence imaging to show the retention of antibodies (Cy5.5-labeled IgG used as a surrogate for aPDL1). Right, semiquantification of the in vivo retention profile. Data are shown as mean \pm s.e.m. ($n = 3$). (b) Average tumor sizes and (c) body weights of mice in different groups. Data are shown as mean \pm s.e.m. ($n = 5$). Statistical significance was calculated by one-way ANOVA with Tukey's post test. * $P < 0.05$; ** $P < 0.01$; *** $P < 0.001$.

induce ICD of cancer cells, we are still interested in exploring the synthesized SN38-SA-BA prodrug in activating the immune system. Herein, we first explored the therapeutic efficacy of SN38 or SN38-SA-BA prodrug to B16F10 cancer cells. As shown by the results of cell viability assay, the cell-killing effect of SN38-SA-BA prodrug was comparable to that of SN38 (Figure 3a). We then investigated the main characteristics of DAMPs in dying cancer cells. As shown in the immunofluorescence staining of cancer cells, obvious exposure of CRT on cancer cell membrane and the release of HMGB1 from nuclei were observed after SN38 or PVA-SN38 hydrogel treatment (Figure 3b-d). Moreover, the quantitative analysis using flow cytometry was further carried out to measure the expression of CRT (Figure 3e) induced by SN38 or PVA-SN38 hydrogel. Meanwhile, it was found that both SN38 and PVA-SN38 could significantly enhance the secretion of ATP by B16F10 cells (Figure 3f). Therefore, considering the efficient immunological cell death induced by the prodrug hydrogel, we supposed that the endogenous ROS in tumor could trigger the release of active SN38, which could further stimulate the production of ROS and trigger the further release of high-dosage SN38.^{24,32} The released SN38 also could induce the ICD of cancer cells, which would promote the antigen presentation by DCs and further activate T-cell-mediated antitumor immune responses (Figure 3g).

Then, we investigated the immune effects mediated by PVA-SN38 hydrogel in vivo. In this experiment, C57B6 mice bearing B16F10 melanoma tumors were intratumorally (i.t.) injected with PBS, PVA & PEG800, free SN38 (228 μ g per mouse), or PVA-SN38 hydrogel (Gel: SN38, 228 μ g per mouse). As shown in the flow cytometry analysis (Figure S3a) and confocal imaging (Figure S3b), the ROS level in the tumor after injected with free SN38 or PVA-SN38 hydrogel was

obviously increased, which was beneficial to the self-accelerated release of SN38. Meanwhile, we studied whether the PVA-SN38 hydrogel could induce the ICD of cancer cells in vivo. Tumors from the mice after i.t. injected with PBS, PVA & PEG800, free SN38, or PVA-SN38 hydrogel were collected and sliced for immunofluorescence staining. As expected, the “eat me” signals, exposure of CRT,^{9,36} and the “danger signal”, release of HMGB1,³⁷ all of which were important for recruitment of DCs and antigen presentation, showed a significant increase in the tumor after PVA-SN38 hydrogel treatment (Figure 4a,b). Moreover, HSP70, an important protein related to DCs maturation and NK cells activation,^{38,39} also showed an obvious increase after PVA-SN38 hydrogel treatment (Figure 4c). Compared to the free SN38 treatment, these danger signals associated with ICD of cancer cells increased after PVA-SN38 hydrogel treatment, possibly ascribing to the controlled and sustained release of the chemotherapeutic drug SN38.

Inspired by the ICD of tumor cells induced by PVA-SN38 hydrogel in vivo, we then investigated different immune cells after PVA-SN38 hydrogel treatment. DCs, a kind of important antigen-presenting cells, play a crucial role in activating the innate and adaptive immune system.¹⁰ To investigate whether the PVA-SN38 hydrogel treatment could accelerate DCs maturation in vivo, C57B6 mice bearing B16F10 tumors were i.t. injected with PBS, PVA & PEG800, free SN38, or PVA-SN38 hydrogel (the dose of SN38 was fixed at 228 μ g per mouse). After 5 days, the mice were sacrificed and their peritumor lymph nodes were obtained and co-stained with anti-CD11c, anti-CD80, and anti-CD86 for flow cytometry assessment. The percentages of matured DCs in those lymph nodes significantly increased after being treated with PVA-SN38 hydrogel, while the DCs maturation from the mice after

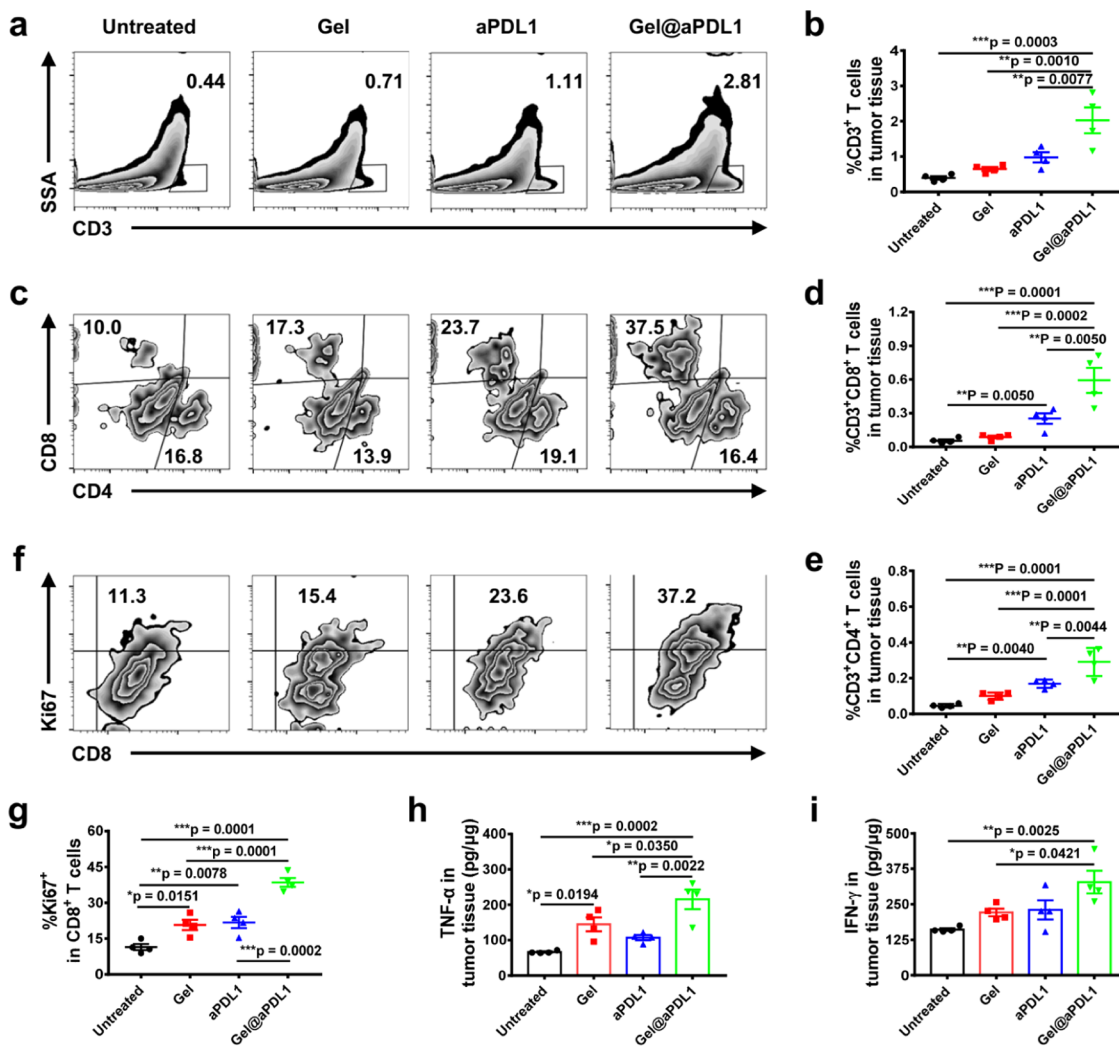


Figure 6. Immune assessment for various treatments. (a–g) Representative FACS plots and the corresponding percentages of (a, b) CD3⁺ T cells, (c, d) CD3⁺CD8⁺ T cells, (c, e) CD3⁺CD4⁺ T cells, and (f, g) CD8⁺Ki67⁺ T cells in the B16F10 tumors. (h, i) The levels of (h) TNF- α and (i) IFN- γ in tumors detected by ELISA. Data are shown as mean \pm s.e.m. ($n = 4$). Statistical significance was calculated by one-way ANOVA with Tukey's post test. * $P < 0.05$; ** $P < 0.01$; *** $P < 0.001$; ns, not significant.

free SN38 treatment showed a moderate increase (Figure 4d). Thus, PVA-SN38 hydrogel treatment could obviously promote DAMPs in melanoma tumors and promote DCs maturation. Meanwhile, other immune cells in the tumor were also measured by flow cytometry. While the percentage of tumor-infiltrating lymphocytes (TILs) (Figure S3c,d) showed no obvious change, the population of immune cells (CD45⁺) (Figure 4e) together with DCs (CD11c⁺) (Figure 4f) obviously increased after PVA-SN38 hydrogel treatment. Thus, compared to the free chemotherapeutic drug, PVA-SN38 hydrogel showed even stronger immune stimulation effect *in vivo*.

3.4. Combination Therapy of Gel@aPDL1. Hydrogel is an ideal drug delivery system that allows a locally controlled and sustainable release of various drugs.²⁹ To explore the potential of PVA-SN38 hydrogel for delivery of immunotherapeutic antibodies, the C57B6 mice bearing tumors were i.t. injected with Cy5.5-labeled IgG (a surrogate for aPDL1) or PVA-SN38 hydrogel encapsulating IgG-Cy5.5, and monitored by the *in vivo* fluorescence imaging system at different time points post-injection. As shown in Figure 5a, while the fluorescence from free IgG-Cy5.5 diminished on day 4, the

fluorescence signals from IgG-Cy5.5 loaded in PVA-SN38 hydrogel still maintained at a high level within the tumor, demonstrating the sustained release of antibodies from hydrogel, which was further confirmed by the semiquantification of fluorescence signals in the tumor.

Next, the therapeutic efficacy of the proposed synergistic chemoimmunotherapy with PVA-SN38 hydrogel enclosed with aPDL1 (Gel@aPDL1) was investigated on the B16F10 melanoma tumor model. Mice bearing B16F10 tumors with average size $\sim 60 \text{ mm}^3$ were randomly divided into four groups: Untreated, Gel (PVA-SN38 hydrogel, SN38: 228 μg per mouse), free aPDL1 (65 μg per mouse, in 30 μL PBS), and Gel@aPDL1 (PVA-SN38 hydrogel encapsulating aPDL1, SN38: 228 μg per mouse; aPDL1: 65 μg per mouse). The growth of tumors was monitored by the caliper every 2 days. As shown in Figure 5b, the blank gel and free aPDL1 only slightly delayed the tumor growth owing to the low dose of SN38 and aPDL1, which is not high enough to cure malignant B16F10 melanoma with one administration. Excitingly, mice injected with Gel@aPDL1 showed remarkable tumor inhibition effects cooperatively. Moreover, the weight of the mice after different treatments exhibited a negligible change,

showing that the local chemoimmunotherapy with hydrogel caused no acute side effects (Figure 5c).

Furthermore, the immune responses after different treatments were investigated in B16F10 tumor model. Tumors were harvested and analyzed using flow cytometry 5 days after different treatments. As shown in Figure 6a,b, compared to the control groups, more CD3⁺ T cells infiltrated into the tumor injected with Gel@aPDL1. More interestingly, the percentage of CD8⁺ T cells, especially Ki67 positive CD8⁺ T cells, which indicated the proliferation or differentiation ability of T cells, significantly increased in the tumor after Gel@aPDL1 treatment, indicating that PDL1 blockade increase the activity of T cells (Figures 6c–g and S4). Then, the intratumor levels of cytokines were examined by ELISA. As shown in Figure 6h, the concentration of TNF- α increased in the tumor after injected with blank gel or Gel@aPDL1, indicating the maturation of DCs and activation of macrophages in TME. Furthermore, the concentration of IFN- γ also significantly increased in the tumor after Gel@aPDL1 treatment (Figure 6i), indicating the effective activation of T lymphocytes after combined chemoimmunotherapy.^{40,41} Finally, the biosafety of this combined chemoimmunotherapy was evaluated and no appreciable abnormality or notable damage was observed in the histological analysis of major organs obtained from mice 30 days after treatment (Figure S5).

4. CONCLUSIONS

In summary, we synthesized the ROS-responsive phenylboronic acid-modified SN38 prodrug SN38-SA-BA, which could be used to cross-link PVA to develop ROS-responsive PVA-SN38 hydrogel for local delivery of aPDL1. In the presence of endogenous ROS within the tumor, SN38-SA-BA could be oxidized and hydrolyzed, leading to the release of chemotherapeutic SN38, which could further promote the generation of ROS and trigger the self-accelerated liberation of SN38, subsequently leading to the degradation of hydrogel with the enhanced release of aPDL1. We have demonstrated that the SN38 prodrug hydrogels could induce ICD of cancer cells, while simultaneously eliciting antitumor immune responses with enhanced infiltration of immune cells. Meanwhile, the released aPDL1 could block the interaction between PD1 and PDL1, increasing the alloreactive T cell population to inhibit the tumor growth. In the mouse melanoma tumor model, PVA-SN38 hydrogel-loaded aPDL1 significantly inhibited the tumor growth. Notably, the ROS-responsive hydrogel could not only serve as a therapeutic reservoir for intratumoral delivery of immunotherapeutics but also enhance the immunogenicity of tumors. Therefore, this injectable ROS-sensitive prodrug-based hydrogel holds promise in increasing the immune responsive rates of ICB to solid tumors.

■ ASSOCIATED CONTENT

SI Supporting Information

The Supporting Information is available free of charge at <https://pubs.acs.org/doi/10.1021/acsami.0c13943>.

Synthesis route of SN38-SA-BA (Scheme S1); gelation of different proportions among PVA, SN38-SA-BA, and PEG800 (Table S1); *in situ* ¹H NMR spectra of SN38-SA-BA (BP) (Figure S1); fabrication of PVA-SN38 hydrogel (Figure S2); immune responses induced by PVA-SN38 hydrogel *in vivo* (Figure S3); percentage of CD8⁺ T cells and CD4⁺ T cells (Figure S4);

biocompatibility of PVA-SN38 hydrogel *in vivo* (Figure S5); ¹H and ¹³C NMR spectra of synthesized compounds (Figures S6–S14); and electrospray ionization high-resolution mass spectra (Figures S15–S18) (PDF)

■ AUTHOR INFORMATION

Corresponding Authors

Jian Sun – Natural Products Research Center, Chengdu Institute of Biology, Chinese Academy of Sciences, Chengdu 610041, Sichuan, P. R. China; University of Chinese Academy of Sciences, Beijing 100049, P. R. China; Email: sunjian@cib.ac.cn

Qian Chen – Institute of Functional Nano & Soft Materials (FUNSOM), Jiangsu Key Laboratory for Carbon-Based Functional Materials & Devices, Soochow University, Suzhou 215123, Jiangsu, P. R. China;  orcid.org/0000-0002-1487-5479; Email: chenqian@suda.edu.cn

Authors

Yimou Gong – Natural Products Research Center, Chengdu Institute of Biology, Chinese Academy of Sciences, Chengdu 610041, Sichuan, P. R. China; University of Chinese Academy of Sciences, Beijing 100049, P. R. China

Muchao Chen – Institute of Functional Nano & Soft Materials (FUNSOM), Jiangsu Key Laboratory for Carbon-Based Functional Materials & Devices, Soochow University, Suzhou 215123, Jiangsu, P. R. China

Yanjun Tan – Institute of Functional Nano & Soft Materials (FUNSOM), Jiangsu Key Laboratory for Carbon-Based Functional Materials & Devices, Soochow University, Suzhou 215123, Jiangsu, P. R. China

Jingjing Shen – Institute of Functional Nano & Soft Materials (FUNSOM), Jiangsu Key Laboratory for Carbon-Based Functional Materials & Devices, Soochow University, Suzhou 215123, Jiangsu, P. R. China

Qiutong Jin – Institute of Functional Nano & Soft Materials (FUNSOM), Jiangsu Key Laboratory for Carbon-Based Functional Materials & Devices, Soochow University, Suzhou 215123, Jiangsu, P. R. China

Wutong Deng – Natural Products Research Center, Chengdu Institute of Biology, Chinese Academy of Sciences, Chengdu 610041, Sichuan, P. R. China

Chao Wang – Natural Products Research Center, Chengdu Institute of Biology, Chinese Academy of Sciences, Chengdu 610041, Sichuan, P. R. China

Zhuang Liu – Institute of Functional Nano & Soft Materials (FUNSOM), Jiangsu Key Laboratory for Carbon-Based Functional Materials & Devices, Soochow University, Suzhou 215123, Jiangsu, P. R. China;  orcid.org/0000-0002-1629-1039

Complete contact information is available at:
<https://pubs.acs.org/10.1021/acsami.0c13943>

Author Contributions

¹Y.G. and M.C. contributed equally to this work. All of the authors have given approval to the final version of the manuscript.

Notes

The authors declare no competing financial interest.

ACKNOWLEDGMENTS

This article was partially supported by the National Research Programs of China (2016YFA0201200), the National Natural Science Foundation of China (91959104, 21927803, 51903182, 51525203), the Natural Science Foundation of Jiangsu Province (BK20190826), Collaborative Innovation Center of Suzhou Nano Science and Technology, and the 111 Program from the Ministry of Education of China.

REFERENCES

- (1) Vyas, D.; Laput, G.; Vyas, A. K. Chemotherapy-Enhanced Inflammation may Lead to the Failure of Therapy and Metastasis. *Oncotargets Ther.* **2014**, *7*, 1015–1023.
- (2) Chen, M. S.; Zhu, X. Y.; Yan, D. Y. Sequential Drug Release for Synergistic Cancer Treatment and Immunity Promotion. *RSC Adv.* **2013**, *3*, 13399–13405.
- (3) Lake, R. A.; Robinson, B. W. S. Immunotherapy and Chemotherapy—a Practical Partnership. *Nat. Rev. Cancer* **2005**, *5*, 397–405.
- (4) Galluzzi, L.; Senovilla, L.; Zitvogel, L.; Kroemer, G. The Secret Ally: Immunostimulation by Anticancer Drugs. *Nat. Rev. Drug Discovery* **2012**, *11*, 215–233.
- (5) Cook, A. M.; Lesterhuis, W. J.; Nowak, A. K.; Lake, R. A. Chemotherapy and Immunotherapy: Mapping the Road Ahead. *Curr. Opin. Immunol.* **2016**, *39*, 23–29.
- (6) Krysko, D. V.; Garg, A. D.; Kaczmarek, A.; Krysko, O.; Agostinis, P.; Vandenabeele, P. Immunogenic Cell Death and DAMPs in Cancer Therapy. *Nat. Rev. Cancer* **2012**, *12*, 860–875.
- (7) Kroemer, G.; Galluzzi, L.; Kepp, O.; Zitvogel, L. Immunogenic Cell Death in Cancer Therapy. *Annu. Rev. Immunol.* **2013**, *31*, 51–72.
- (8) Garg, A. D.; Agostinis, P. Cell Death and Immunity in Cancer: from Danger Signals to Mimicry of Pathogen Defense Responses. *Immunol. Rev.* **2017**, *280*, 126–148.
- (9) Obeid, M.; Tesniere, A.; Ghiringhelli, F.; Fimia, G. M.; Apetoh, L.; Perfettini, J.-L.; Castedo, M.; Mignot, G.; Panaretakis, T.; Casares, N.; Metivier, D.; Larochette, N.; van Endert, P.; Ciccosanti, F.; Piacentini, M.; Zitvogel, L.; Kroemer, G. Calreticulin Exposure Dictates the Immunogenicity of Cancer Cell Death. *Nat. Med.* **2007**, *13*, 54–61.
- (10) Wculek, S. K.; Cueto, F. J.; Mujal, A. M.; Melero, I.; Krummel, M. F.; Sancho, D. Dendritic Cells in Cancer Immunology and Immunotherapy. *Nat. Rev. Immunol.* **2020**, *20*, 7–24.
- (11) Feng, B.; Zhou, F.; Hou, B.; Wang, D.; Wang, T.; Fu, Y.; Ma, Y.; Yu, H.; Li, Y. Binary Cooperative Prodrug Nanoparticles Improve Immunotherapy by Synergistically Modulating Immune Tumor Microenvironment. *Adv. Mater.* **2018**, *30*, No. e1803001.
- (12) Vanmeerbek, I.; Sprooten, J.; De Ruysscher, D.; Teijpar, S.; Vandenberghe, P.; Fucikova, J.; Spisek, R.; Zitvogel, L.; Kroemer, G.; Galluzzi, L.; Garg, A. D. Trial Watch: Chemotherapy-Induced Immunogenic Cell Death in Immuno-oncology. *Oncoimmunology* **2020**, *9*, No. e1703449.
- (13) Mizumoto, N.; Gao, J. M.; Matsushima, H.; Ogawa, Y.; Tanaka, H.; Takashima, A. Discovery of Novel Immunostimulants by Dendritic-Cell-Based Functional Screening. *Blood* **2005**, *106*, 3082–3089.
- (14) Li, Q. Y.; Zu, Y. G.; Shi, R. Z.; Yao, L. P. Review Camptothecin: Current Perspectives. *Curr. Med. Chem.* **2006**, *13*, 2021–2039.
- (15) Tanaka, H.; Matsushima, H.; Mizumoto, N.; Takashima, A. Classification of Chemotherapeutic Agents Based on Their Differential In vitro Effects on Dendritic Cells. *Cancer Res.* **2009**, *69*, 6978–6986.
- (16) Ma, W.; Su, H.; Cheetham, A. G.; Zhang, W. F.; Wang, Y. Z.; Kan, Q. C.; Cui, H. G. Synergistic Antitumor Activity of a Self-assembling Camptothecin and Capecitabine Hybrid Prodrug for Improved Efficacy. *J. Controlled Release* **2017**, *263*, 102–111.
- (17) Zhou, Q.; Shao, S. Q.; Wang, J. Q.; Xu, C. H.; Xiang, J. J.; Piao, Y.; Zhou, Z. X.; Yu, Q. S.; Tang, J. B.; Liu, X. R.; Gan, Z. H.; Mo, R.; Gu, Z.; Shen, Y. Q. Enzyme-activatable Polymer-drug Conjugate Augments Tumour Penetration and Treatment Efficacy. *Nat. Nanotechnol.* **2019**, *14*, 799–811.
- (18) Rubinfeld, B.; Upadhyay, A.; Clark, S. L.; Fong, S. E.; Smith, V.; Koeppen, H.; Ross, S.; Polakis, P. Identification and Immunotherapeutic Targeting of Antigens Induced by Chemotherapy. *Nat. Biotechnol.* **2006**, *24*, 205–209.
- (19) Wei, J.; DeAngulo, G.; Sun, W.; Hussain, S. F.; Vasquez, H.; Jordan, J.; Weinberg, J.; Wolff, J.; Koskina, N.; Heimberger, A. B. Topotecan Enhances Immune Clearance of Gliomas. *Cancer Immunol. Immunother.* **2009**, *58*, 259–270.
- (20) Sharma, A.; Lee, M.-G.; Won, M.; Koo, S.; Arambula, J. F.; Sessler, J. L.; Chi, S.-G.; Kim, J. S. Targeting Heterogeneous Tumors Using a Multifunctional Molecular Prodrug. *J. Am. Chem. Soc.* **2019**, *141*, 15611–15618.
- (21) Sharma, P.; Allison, J. P. The Future of Immune Checkpoint Therapy. *Science* **2015**, *348*, 56–61.
- (22) Chen, Q.; Xu, L.; Liang, C.; Wang, C.; Peng, R.; Liu, Z. Photothermal Therapy with Immune-Adjuvant Nanoparticles Together with Checkpoint Blockade for Effective Cancer Immunotherapy. *Nat. Commun.* **2016**, *7*, No. 13193.
- (23) Kyi, C.; Postow, M. A. Immune Checkpoint Inhibitor Combinations in Solid Tumors: Opportunities and Challenges. *Immunotherapy* **2016**, *8*, 821–837.
- (24) Wang, C.; Wang, J. Q.; Zhang, X. D.; Yu, S. J.; Wen, D.; Hu, Q. Y.; Ye, Y. Q.; Bomba, H.; Hu, X. L.; Liu, Z.; Dotti, G.; Gu, Z. In situ formed Reactive Oxygen Species-responsive Scaffold with Gemcitabine and Checkpoint Inhibitor for Combination Therapy. *Sci. Transl. Med.* **2018**, *10*, No. eaan3682.
- (25) Chen, Q.; Chen, G.; Chen, J.; Shen, J.; Zhang, X.; Wang, J.; Chan, A.; Gu, Z. Bioresponsive Protein Complex of aPD1 and aCD47 Antibodies for Enhanced Immunotherapy. *Nano Lett.* **2019**, *19*, 4879–4889.
- (26) Alsaab, H. O.; Sau, S.; Alzhrani, R.; Tatiparti, K.; Bhise, K.; Kashaw, S. K.; Iyer, A. K. PD-1 and PD-L1 Checkpoint Signaling Inhibition for Cancer Immunotherapy: Mechanism, Combinations, and Clinical Outcome. *Front. Pharmacol.* **2017**, *8*, 561.
- (27) Wakabayashi, G.; Lee, Y. C.; Luh, F.; Kuo, C. N.; Chang, W. C.; Yen, Y. Development and Clinical Applications of Cancer Immunotherapy Against PD-1 Signaling Pathway. *J. Biomed. Sci.* **2019**, *26*, 96.
- (28) Seidel, J. A.; Otsuka, A.; Kabashima, K. Anti-PD-1 and anti-CTLA-4 Therapies in Cancer: Mechanisms of Action, Efficacy, and Limitations. *Front. Oncol.* **2018**, *8*, 86.
- (29) Croisfelt, F. M.; Tundisi, L. L.; Ataide, J. A.; Silveira, E.; Tambourgi, E. B.; Jozala, A. F.; Souto, E. M. B.; Mazzola, P. G. Modified-Release Topical Hydrogels: A Ten-Year Review. *J. Mater. Sci.* **2019**, *54*, 10963–10983.
- (30) Chen, Q.; Chen, M.; Liu, Z. Local Biomaterials-assisted Cancer Immunotherapy to Trigger Systemic Antitumor Responses. *Chem. Soc. Rev.* **2019**, *48*, 5506–5526.
- (31) Chao, Y.; Chen, Q.; Liu, Z. Smart Injectable Hydrogels for Cancer Immunotherapy. *Adv. Funct. Mater.* **2020**, *30*, No. 1902785.
- (32) Zhang, W. J.; Hu, X. L.; Shen, Q.; Xing, D. Mitochondria-specific Drug Release and Reactive Oxygen Species Burst Induced by Polyprodrug Nanoreactors can Enhance Chemotherapy. *Nat. Commun.* **2019**, *10*, No. 1704.
- (33) Xie, C.; Yang, C. C.; Zhang, P.; Zhang, J. L.; Wu, W.; Jiang, X. Q. Synthesis of Drug-crosslinked Polymer Nanoparticles. *Polym. Chem.* **2015**, *6*, 1703–1713.
- (34) Cromwell, O. R.; Chung, J.; Guan, Z. Malleable and Self-Healing Covalent Polymer Networks through Tunable Dynamic Boronic Ester Bonds. *J. Am. Chem. Soc.* **2015**, *137*, 6492–6495.
- (35) Meng, Z.; Zhou, X.; Xu, J.; Han, X.; Dong, Z.; Wang, H.; Zhang, Y.; She, J.; Xu, L.; Wang, C.; Liu, Z. Light-Triggered In Situ Gelation to Enable Robust Photodynamic-Immunotherapy by Repeated Stimulations. *Adv. Mater.* **2019**, *31*, No. 1900927.
- (36) Panaretakis, T.; Kepp, O.; Brockmeier, U.; Tesniere, A.; Bjorklund, A.-C.; Chapman, D. C.; Durchschlag, M.; Jozala, N.; Pierron, G.; van Endert, P.; Yuan, J.; Zitvogel, L.; Madeo, F.; Williams, D. B.;

Kroemer, G. Mechanisms of Pre-apoptotic Calreticulin Exposure in Immunogenic Cell Death. *EMBO J.* **2009**, *28*, 578–590.

(37) Lee, J.-J.; Park, I. H.; Rhee, W. J.; Kim, H. S.; Shin, J.-S. HMGB1 Modulates the Balance Between Senescence and Apoptosis in Response to Genotoxic Stress. *FASEB J.* **2019**, *33*, 10942–10953.

(38) Nishikawa, M.; Takemoto, S.; Takakura, Y. Heat Shock Protein Derivatives for Delivery of Antigens to Antigen Presenting Cells. *Int. J. Pharm.* **2008**, *354*, 23–27.

(39) Multhoff, G. Activation of Natural Killer Cells by Heat Shock Protein 70. *Int. J. Hyperthermia* **2009**, *25*, 169–175.

(40) Cheng, B. B.; Yuan, W. E.; Su, J.; Liu, Y.; Chen, J. J. Recent Advances in Small Molecule Based Cancer Immunotherapy. *Eur. J. Med. Chem.* **2018**, *157*, 582–598.

(41) Fridman, W. H.; Zitvogel, L.; Sautes-Fridman, C.; Kroemer, G. The Immune Contexture in Cancer Prognosis and Treatment. *Nat. Rev. Clin. Oncol.* **2017**, *14*, 717–734.